Image Log Interpretation and Geomechanical Issues

Troyee Dasgupta, Swagato Dasgupta and Soumyajit Mukherjee

Abstract Structural geological texts, research papers and books, are progressively incorporating well logging-related studies and geomechanical issues, including borehole imaging techniques. Geomechanical studies usually involve magnitudes and orientations of the three principal stress axes: S_v—vertical stress, and S_{hmin} and S_{Hmax}—the minimum and the maximum horizontal stresses, respectively. Electrical, acoustic or video devices that capture high-resolution images are lowered into the well and give crucial information about bed boundaries, structural elements such as faults, folds, discontinuities, fractures and even secondary porosities such as fractures and vugs. Image log data gives important information about the S_{hmin} and S_{Hmax} directions. Hoop stresses acting along the circumference of the borehole wall causes breakouts, and the radial stresses result in tensile fractures known as drilling-induced fractures. Borehole breakouts and drilling-induced fractures can be easily distinguished with the help of borehole images. By integrating the information obtained from image logs and other kinds of well logs, one can get orientations of the minimum and maximum horizontal stresses. We present two problems, relevant to classroom teaching for geoscience students, and solutions related to geomechanical issues and image log interpretation.

Keywords Geomechanics · Stress regimes · Image log · Borehole breakouts Drilling-induced fractures

T. Dasgupta
Exploration Division, Reliance Industries Ltd., Navi Mumbai 400701, Maharashtra, India

S. Dasgupta · S. Mukherjee (✉)
Department of Earth Sciences, Indian Institute of Technology Bombay, Powai, Mumbai 400 076, Maharashtra, India
e-mail: soumyajitm@gmail.com; smukherjee@iitb.ac.in

S. Mukherjee (ed.), *Teaching Methodologies in Structural Geology and Tectonics*, Springer Geology, https://doi.org/10.1007/978-981-13-2781-0_10

1 Introduction

Tectonic stresses act along the Earth's surface as well as within the crust. The magnitudes of stresses depend upon factors such as geological processes, depth, pore pressure, frictional coefficient and rock strength (Zoback 2007). Thus, geomechanical issues have become subjects of active interest in structural geology and tectonics (Zoback et al. 1985; Barton and Zoback 2002; Nelson et al. 2005; Fowler and Weir 2008; Mukherjee 2013; Richardson et al. 2015; Fossen 2016; Mulchrone and Mukherjee 2016).

To address geomechanical problems in oil and gas industries as well as geothermal reservoirs, knowledge about the local and the regional stresses is required (Zoback 2007; Fellgett et al. 2018). Anderson's (1905) scheme is helpful in understanding the relative magnitudes of highest, intermediate and minimum stresses (σ_1, σ_2 and σ_3, respectively) in terms of different stress regimes where normal, strike-slip and reverse faulting are preferred. The stress magnitudes in the three end-member regimes can also be explained in terms of vertical overburden stress (S_v) and the maximum and minimum horizontal stresses (S_{Hmax} and S_{hmin}; Fig. 1). In this model, $S_v = \sigma_1$ is for normal faults, $S_v = \sigma_2$ for strike-slip faults and $S_v = \sigma_3$ for reverse faults. Under most geological conditions, the principal stresses are compressional rather than tensile (e.g. Fossen 2016). The convention amongst structural geologists is to define stress as positive in compression.

There are several techniques for measuring in situ stresses. The parameters for stress estimation can be deduced from the following procedures to get an overview of stress orientations (Zoback 2007).

I. The vertical stress (S_v), due to the overburden pressure, can be estimated from a density log.

II. S_{hmin} can be obtained during well drilling operations from procedures such as leak-off tests (LOT) and hydro-fracturing techniques such as the mini-frac test.

A mini-frac is a type of small fracturing test usually performed before the key hydraulic fracturing test. It provides important information regarding the response of the tested interval, geometry and propagation of hydro-fractures and the magnitude of S_{hmin} (De Bree and Walters 1989; Zoback 2007).

III. Pore pressure (P_p) can be estimated directly from conventional logs in real time while drilling a well or can be inferred from seismic velocities while defining a pre-drill pore-pressure model. The estimated pore pressure can be calibrated with actual pore fluid pressure data obtained from reservoir sand bodies.

IV. Estimates of S_{Hmax} and S_{hmin} orientations can be obtained from borehole breakouts as well as drilling-induced fracture studies from image logs.

V. To obtain stress magnitudes, information about rock properties is required. Rock strength can be measured from laboratory-based rock compressibility tests. It can also be estimated from density and sonic *P*-wave and *S*-wave logs.

The rock failure can be explained with the Mohr–Coulomb failure criteria (Zoback 2007; Labuz and Zang 2012) where the knowledge of two parameters, viz. μ_i—coefficient of internal friction, and Co or UCS—unconfined compressive

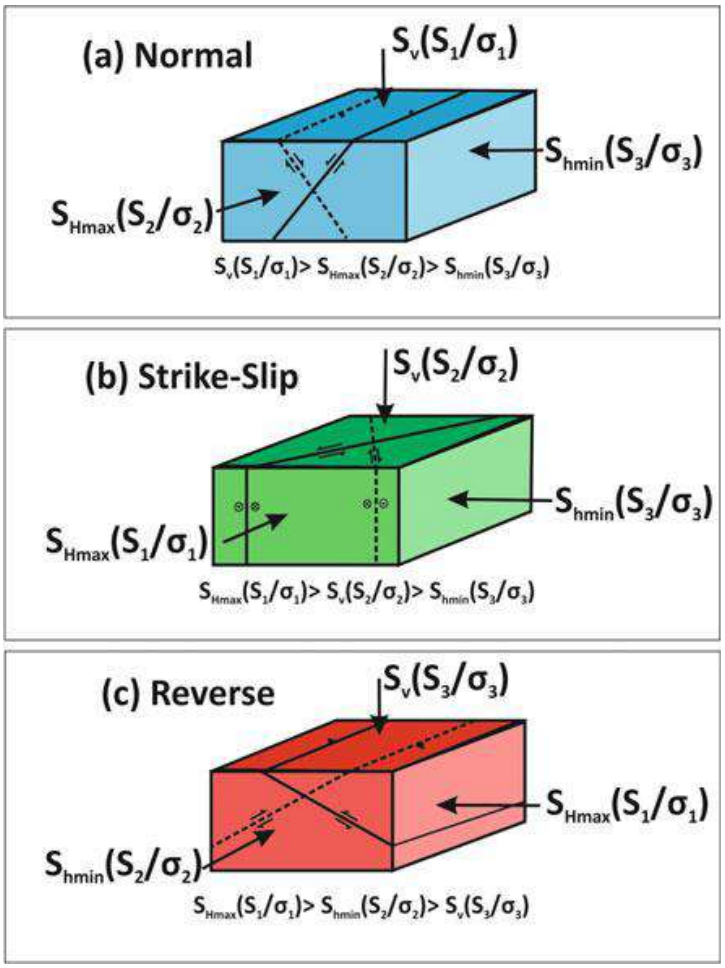

Fig. 1 Three modes of Andersonian faulting mechanism in extensional, strike-slip and compressional regime

strength, is required. As the Mohr circle touches the failure envelope, depending on the magnitude of maximum and minimum principal stresses, shear failure, tensile failure or hybrid failure of the rock may take place. The rock is in the stability field below the failure envelope, which is defined by:

$$\left(S_{\mathrm{Hmax}} - P_{\mathrm{p}}\right) / \left(S_{\mathrm{hmin}} - P_{\mathrm{p}}\right) = \left[\sqrt{\left(\mu^2 + 1\right)} + \mu\right]^2 \tag{1}$$

The above equation can be rewritten in the following forms for different stress regimes

$$\text{Reverse fault regime}: \left(S_{\mathrm{Hmax}} - P_{\mathrm{p}}\right) / \left(S_v - P_p\right) = \left[\sqrt{\left(\mu^2 + 1\right)} + \mu\right]^2 \tag{2}$$

$$\text{Normal fault regime}: \left(S_{\mathrm{v}} - P_{\mathrm{p}}\right) / \left(S_{\mathrm{hmin}} - P_{\mathrm{p}}\right) = \left[\sqrt{\left(\mu^2 + 1\right)} + \mu\right]^2 \tag{3}$$

$$\text{Strike slip fault regime}: \left(S_{\mathrm{Hmax}} - P_{\mathrm{p}}\right) / \left(S_{\mathrm{hmin}} - P_{\mathrm{p}}\right) = \left[\sqrt{\left(\mu^2 + 1\right)} + \mu\right]^2 \tag{4}$$

The magnitude of μ generally ranges from 0.6 to 1 (Byerlee 1978; Zoback 2007).

Image logs can be integrated with other data such as wireline logs, core data and production data to give detailed information about the geology (Hurley 2004).

Modern-day logging tools can retrieve image logs created by high-intensity sensors (sensors having higher strength) that pick up samples both horizontally and vertically. Resistivity-based image tools consist of four or six arm calipers. Each arm is equipped with pads in which micro-resistivity electrodes are placed that acts as sensors. These pads get pressed against the borehole wall for recording image data around the borehole (OBMI brochure: Schlumberger 2006). Thus, samples consist of image data defined by resistivity contrast representing lithological and structural variations. This high-resolution sampling of data creates images that give a continuous record of the formation and the borehole circumference (Rider 2011).

Generally, 40–80% of the borehole information is covered by image logs and the best images are obtained in case of resistivity-derived electrical images when the resistivity ratio between the mud and the formation is <1000 (Hurley 2004). At first, optical photography was performed using a 16 mm lens by Birdwell in 1964. Shell first used downhole black and white television camera. Later, there was an evolution of logs from optical to acoustic to finally electrical image logs (Prensky 1999).

Nowadays, conventional coring of wells is costly affairs. In some lithologies, e.g. in unconsolidated sands and brecciated rocks in deformation/fault zones, the core recovery is poor and the chances of losing critical information of the well are high. In these circumstances, subsurface sedimentological and structural data are obtained by imaging techniques by these advanced logging tools. Therefore, such tools have become popular in the recent years (Hurley 2004).

This chapter will discuss deciphering structural features such as breakouts and drilling-induced fractures from image logs, and the usefulness of these features in deducing the maximum and minimum horizontal stress directions.

2 Image Logging Tools

Imaging tools are broadly of two categories that perform either electrical or acoustic imaging. The electrical borehole tools are the most sophisticated and commercially available tools (Hurley 2004). Image log tools are generally equipped with pads and are pressed against the borehole wall when lowered. Button electrodes (current and voltage electrodes) are embedded in the pads of the tools where the potential difference is measured between the voltage electrodes at the centre of the pad face (OBMI brochure—Schlumberger 2006). The effective button size and effective resolution are 0.2 in. and 1.2 in., respectively, and the depth of investigation is 3.5 in. These tools have 32% coverage of the borehole—this is the general working principle of an image tool working in the non-conductive borehole environment (OBMI brochure—Schlumberger 2006).

In case of boreholes drilled with water-based mud, the image log tool has a specification to cover 80% of the 8 in. hole and the button size is of 0.2 in. with a vertical as well as horizontal resolution of 0.2 in. Because of the micro-resistivity changes resulted by the passage of the current in the rock, we get images and

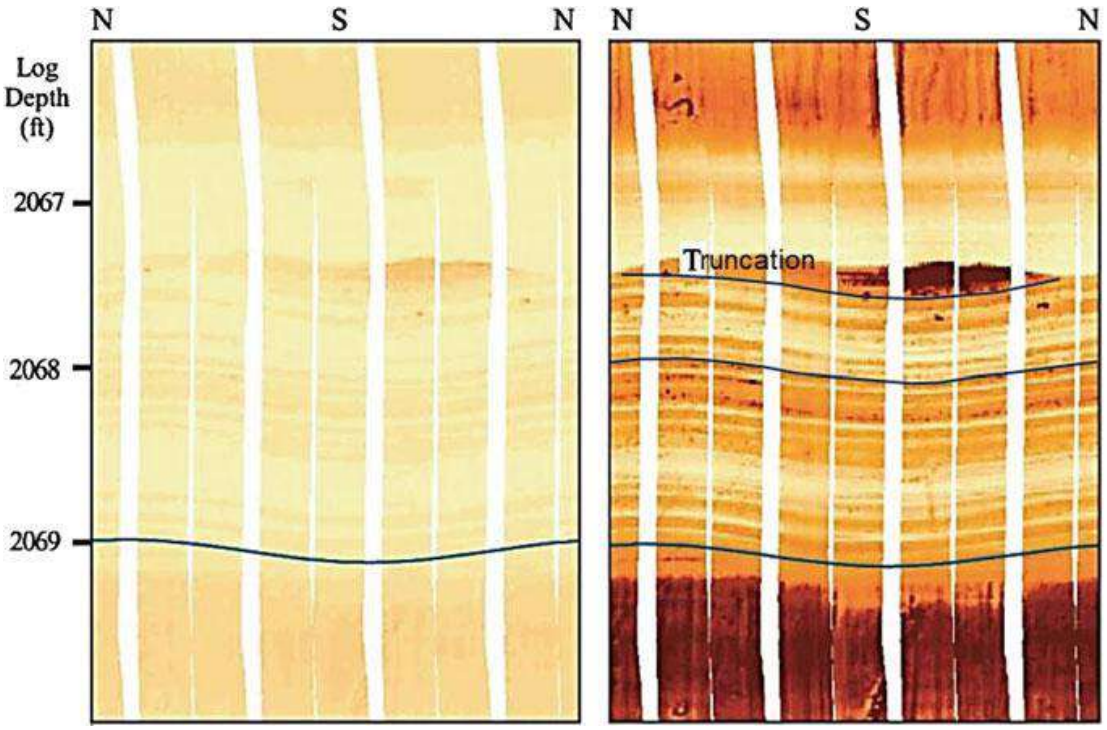

Fig. 2 Comparison between static (left) and dynamic image (right) of a massive sandstone. The truncated surface, as highlighted by 'Truncation', and finer laminations are also visible. Dynamic processing is done in a moving window of 5 ft and the geological features are prominent in this image. N-S-N refers to the true north reference. Modified after Hurley (2004)

these are interpreted as textural features, stratigraphic and structural features (FMI brochure—Schlumberger 2002).

After the data acquisition, the array data is processed with necessary corrections. Two images in the unwrapped borehole formats are generated: static and dynamic (Fig. 2). In the static image, a colour contrast is applied to the entire well. On the other hand, in the dynamic image, the colour contrast is applied to a specific moving window length. Dynamic images help to identify subtle features, e.g. vugs, bed boundaries, low resistivity shales, fractures and other geological features (Hurley 2004).

Apart from the wireline imaging, logging while drilling (LWD) imaging tools are also available. The two common varieties are: resistivity at bit (RAB, Schlumberger) and StarTrak (Baker Hughes). In acoustic imaging tools, rotating transducers exist, which emit and record sound waves and these tools are often referred to as the "borehole televiewers" (Rider 2011; Hurley 2004). These tools were first developed in the 1960s by Mobil, and later several oil companies improved them. The amplitude and travel time are recorded and processed as images through these tools. The acoustic borehole imaging tools are summarized in Appendix-2 (Rider 2011; Hurley 2004; Tingay et al. 2008)

3 Image Log Interpretation

Nowadays, image logs are interpreted in workstations, where both static and dynamic images are studied by the log analysts. Features such as bed boundaries and natural fractures are picked by the interpreter by fitting sine curves. Automated dip picking is done by certain algorithms. The dip picking can be edited and interpreted manually when required. Image logs can also identify stress-induced fractures such as breakouts and drilling-induced fractures, which is the main focus of this chapter.

To optimize the wellbore design, the knowledge of in situ stresses and the compressive strength of the (anisotropic) rocks is required (Chatterjee and Singha 2018). Understanding local and regional stresses is important as these can produce and propagate hydraulic fractures. Knowing stress regimes is important in petroleum exploration projects such as in the deep-water gas hydrate exploration and in integrated ocean drilling programmes (IODP).

In tight reservoirs, flow of hydrocarbon is enabled by creating hydraulic fractures through stimulations (Bailey et al. 2017). Local and regional stresses control the generation of these fractures (Bell 1996; Hillis and Reynolds 2000; Bailey et al. 2017).

The main components of stresses as discussed above are S_v (principal vertical stress), S_{Hmax} (maximum horizontal stress) and S_{hmin} (minimum horizontal stress). The orientation of S_{Hmax} plays an important role in petroleum industry and can be obtained from borehole breakouts and drilling-induced fractures (Zoback 1992; Bell 1996; Rajabi et al. 2017). Borehole breakouts happen perpendicular to the S_{Hmax}. On the other hand, drilling-induced fractures are parallel to the S_{Hmax} direction, i.e. orthogonal to S_{hmin} (Zoback 2007; Fowler and Weir 2008; Tingay et al. 2008; Rajabi et al. 2017). In the subsequent sections, the formation of breakout and drilling-induced fracture process will be explained.

Borehole breakouts: Borehole breakout was classically described by Bell and Gough (1979) and Gough and Bell (1981). Later, Zoback et al. (1985) expanded the study theoretically along with several experiments. Stress-induced deformation can result in borehole breakouts that occur in a preferential direction when the stress concentration around the borehole exceeds the rock strength (Zoback et al. 1985; Fowler and Weir 2008). Breakouts are the wellbore enlargements, which propagates in conical geometry, seen as spalled regions, and form where the circumferential stress ($\sigma_{\Theta\Theta}$) around the borehole exceeds the rock strength (Lai et al. 2018). Spalling occurs in the direction of minimum horizontal stresses (S_{hmin}) in breakouts (Fig. 3; Thorsen 2011). Studies on breakouts provide information about the stress field orientations. Elastic models indicate that the breakouts are the result of compressive failure as per the Mohr–Coulomb failure criteria (Zoback et al. 1985; Zoback 2007). The stress around the wellbore is explained by circumferential stress ($\sigma_{\Theta\Theta}$).

Bell (2003) discusses a few points about the reliability of the S_{hmin} direction from breakout study: (i) several breakouts encountered in a well can constrain the stress orientation; (ii) the drilled well must be vertical or have up to 3° inclination. Borehole breakout interpretations need to be performed very carefully, since in many cases

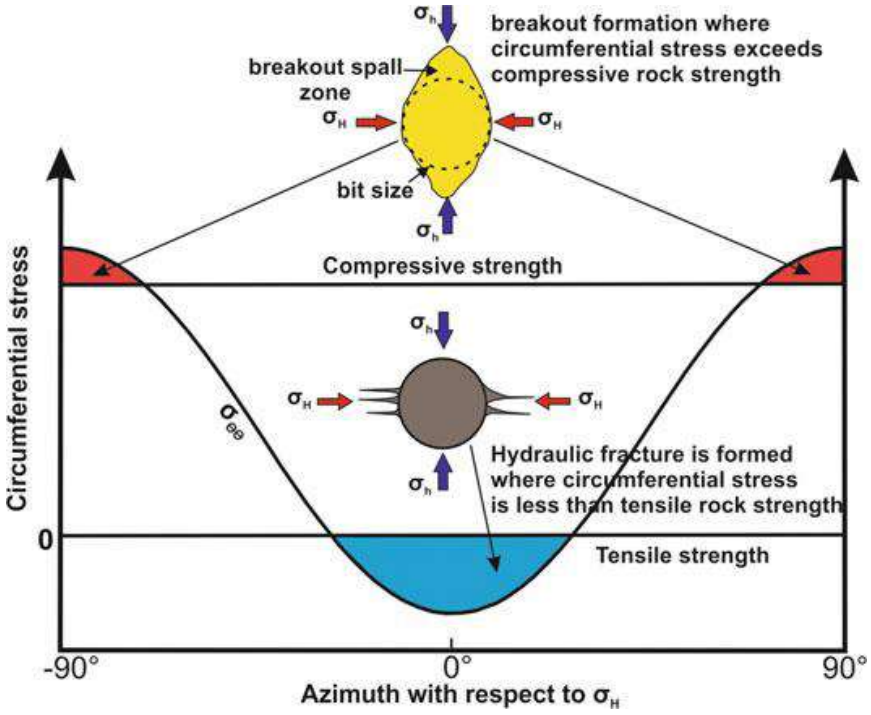

Fig. 3 Schematic cross-section of well bore showing formation of breakouts and hydraulic fractures. The figure shows the variation of circumferential stress ($\sigma_{\Theta\Theta}$) to azimuth. Modified after Hillis and Reynolds (2000)

the long axis of the breakout could be due to the result of key seating by abrasion on one side of the wall in consequence to lowering of the drilling equipment (Fig. 2a, b; Bell 2003).

In order to understand stress concentration around a vertical borehole wall, principal stresses are transformed from an orthogonal system to a cylindrical system in which case they act parallel and perpendicular to borehole wall.

At any point around the wellbore, the stresses (Zoback 2007) can be described as:

I. Radial stress (σ_{rr}) acts along the radius of the wellbore. It is the difference between wellbore pressure and pore pressure acting radially along the wellbore.

II. Hoop stress or circumferential stress ($\sigma_{\Theta\Theta}$) acts around the wellbore circumference. It depends on several factors such as the wellbore pressure, magnitude and orientation of stress, hole inclination and azimuth and the pore pressure of the formation.

III. Axial stress (σ_{zz}) acts parallel to the well path and is not affected by the mud weight. σ_{zz} depends on the in situ stress and its orientation and magnitude, hole inclination and azimuth, pore pressure, etc. When a well is vertically drilled with $S_{Hmax} = S_{hmin}$, the axial stress equals the vertical stress. For an inclined well, this relation will not hold true.

The degree of breakout varies in rocks: in crystalline rocks, it appears as small chips and usually initiates from the borehole wall. On the other hand, in sedimentary rocks, it initiates as fractures within the formation (Fowler and Weir 2008). The breakout lengths range from <1 m up to tens of m.

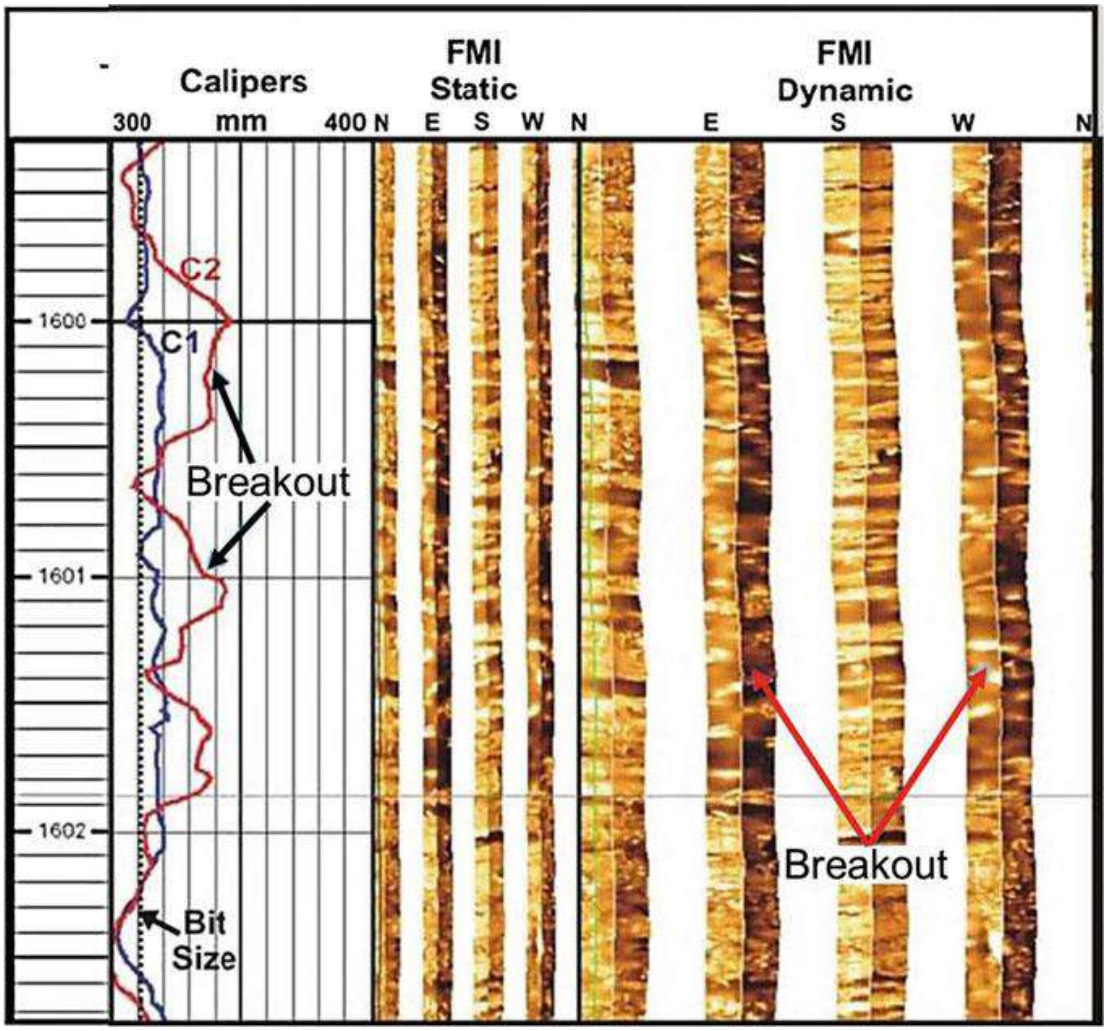

Fig. 4 Borehole breakouts interpreted on a FMI (formation micro imager log). The caliper 2 directions (C2 marked in red) show borehole enlargement feature and the FMI log directly shows broad poorly resolved conductive zones. These borehole breakout features are oriented towards 100ºN and 290ºN and display ~N–S oriented S_{Hmax} (from Tingay et al. 2008)

Borehole breakouts can be directly identified from electrical images depending on the contrast in resistivity. In resistivity images, breakouts appear as broad, conductive zones with poor resolution and these are usually parallel and 180° apart in either static or dynamic images, and are accompanied by enlarged caliper features (Tingay et al. 2008; Rajabi et al. 2017). Breakout appears as resistive features in images generated by the Oil-based Micro Imager (OBMI; Fig. 4).

Borehole breakout can easily be interpreted using the acoustic images. Breakouts are prominent features in both amplitudes and borehole radius (travel time) data of the acoustic images. As the borehole breakouts have typically rough surfaces, they appear as broad low amplitude zones with increased travel time on opposite sides of borehole (Tingay et al. 2008; Fig. 5). As per Zoback (2007), the most reliable way to analyse breakouts is through ultrasonic image logs where the breakouts appear as dark bands with low reflectance images on opposite sides of the wellbore. Breakout

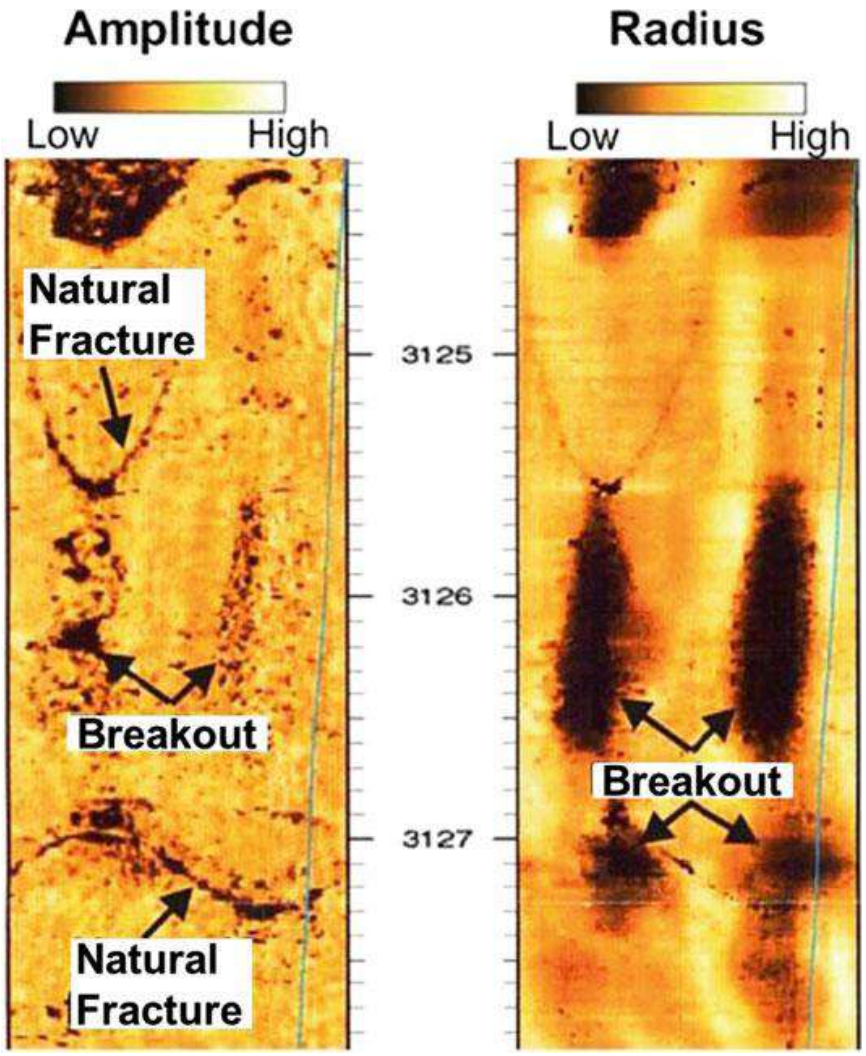

Fig. 5 Borehole breakout and drilling-induced fracture observed on acoustic image log. Borehole breakouts are identified as broader zones with high radius and low reflection amplitude and oriented around 095–275 N. The breakouts indicate that the present day maximum horizontal stress (σ_{Hmax}) trends N–S (from Tingay et al. 2008)

may appear as en echelon features in oil-based mud (OBM) with respect to the breakouts in water-based mud (WBM) (Fig. 4c, d; Nian et al. 2016).

Drilling-induced fractures: In gas, oil and geothermal wells, drilling-induced fractures are commonly present as there is concentration of far-field stresses close to the borehole and these stresses commonly exceed the strength of the rock (Barton and Zoback 2002). In four or six arm caliper image logs, natural fractures can be seen as a feature that cut across the wellbore (as in Dasgupta et al. 2018), whereas the drilling-induced fractures (DIFs) appear as subparallel to wellbore axis (i.e. vertical) or slightly dipping features in vertical wells (Fig. 6; Tingay et al. 2008). DIFs usually appear as narrow resistive features in the OBMI as well as conductive features in image logs and are 180° apart (Tingay et al. 2008; Lai et al. 2018). Drilling-induced fractures form when the circumferential stress exceeds the tensile strength of the rock

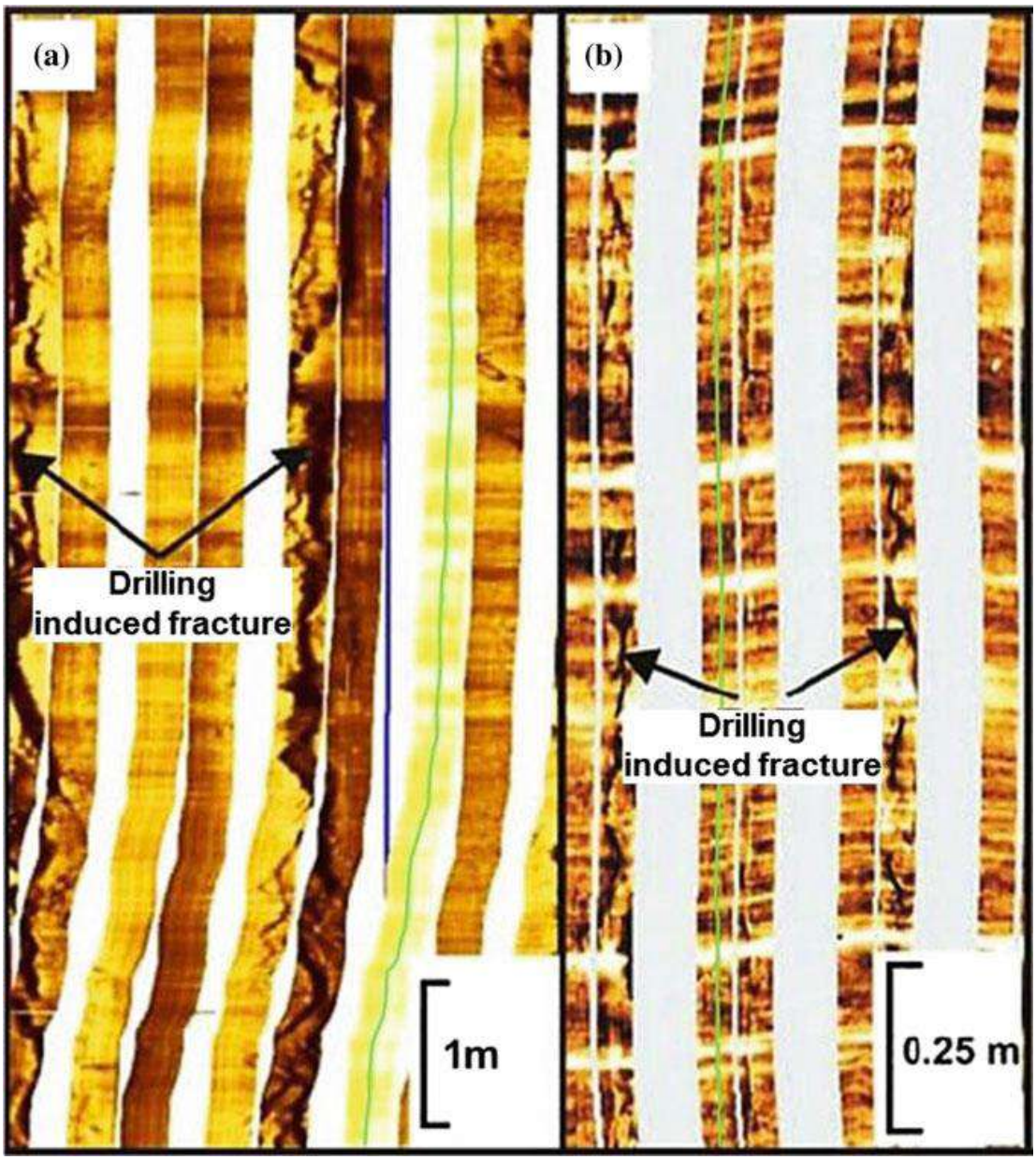

Fig. 6 DIFs interpreted from image Formation Micro Imager logs (FMI). These are seen as 180° apart conductive narrow features. **a** DIFs trending 010–190ºN indicates N–S oriented maximum horizontal stress (σ_{Hmax}). **b** DIFs orient towards 040 and 220ºN. NE–SW is the approximately the maximum horizontal stress direction (σ_{Hmax}) (Reproduced from Tingay et al. 2008)

and are oriented along the S_{Hmax} (Tingay et al. 2008). The most valuable information obtained by studying drilling-induced fractures is the determination of stress fields, which is worked out routinely in oil and gas fields (Barton and Zoback 2002).

Peska and Zoback (1995) demonstrate that apart from occurrence of drilling-induced fractures occurring in significant wellbore—fluid overpressure conditions—there are various other reasons of fracturing. Generally in vertical boreholes, the drilling-induced fractures parallel S_{Hmax}. In deviated wells, these fractures appear as en echelon features (Fig. 1b; Barton and Zoback 2002).

Image logs are to be interpreted carefully as the drilling-induced fractures and drilling-enhanced natural fractures (Fig. 3a, Barton and Zoback 2002) can resemble each other morphologically. The only way to distinguish is that drilling-induced fractures are discontinuous whereas the drilling-enhanced natural fractures can be picked as sinusoidal curves.

3.1 Problems

Question 1:

Fig. 7 is an image log of a formation where the four pads of the tool show some distinct features. The darker colour represents conductive layers and the lighter colour the resistive ones. Parallel laminations are distinct. Feature 2 is a prominent characteristic observed in pads 1 and 3, whereas feature 1 can be seen in pad 3 and pad 4. Identify these two features.

Answer:

Feature 1 is a signature that is broad and presumably blurred. Feature 1 is a breakout. Feature 2 is linear and runs parallel in two pads. Feature 2 is drilling-induced fracture. The geoscientist should be able to distinguish non-tectonic or atectonic structures from tectonic ones. From this example, it is observed that the S_{Hmax} is oriented along the pads 1 and 3, whereas S_{hmin} is oriented along the pads 2 and 4. Since no en echelon fractures are seen, whether the image log is from a vertical well cannot be commented. Note the answer is independent to location of borehole and the stress state. The identified features do not specify any tectonic/stress regime: extensional, compressional and strike-slip.

Question 2:

a. Consider two different stress regimes: compressive—reverse fault regime and extensional—normal fault regime, where the overburden pressure, pore pressure and coefficient of internal friction are the same. The overburden pressure (S_{v}) at 3210 m depth is 88.5 MPa with an in situ pore pressure ~31 MPa. Taking the coefficient of internal friction (μ) = 0.6, find out the magnitude of the σ_{Hmax}, in case of reverse fault regime, and the σ_{hmin}, in case of normal fault regime.

b. At 2500 m depth, the overburden stress (S_{v}) is 70 MPa. The minimum compressive stress (S_{hmin}) deduced from leak-off test is 61.5 MPa. At a certain pore pressure, estimate the possible range of S_{Hmax} without performing any calculations. Also, deduce the possible stress regime. Knowing stress regime helps in wellbore stability and predicting induced fracturing. The hydraulic fracture orientation is controlled by the local stress regime. For example, hydraulic fracture forms on a vertical plane for a normal and a strike-slip fault regime. On the other hand, hydraulic fracture forms in a horizontal plane when a reverse fault regime prevails (Lin et al. 2008).

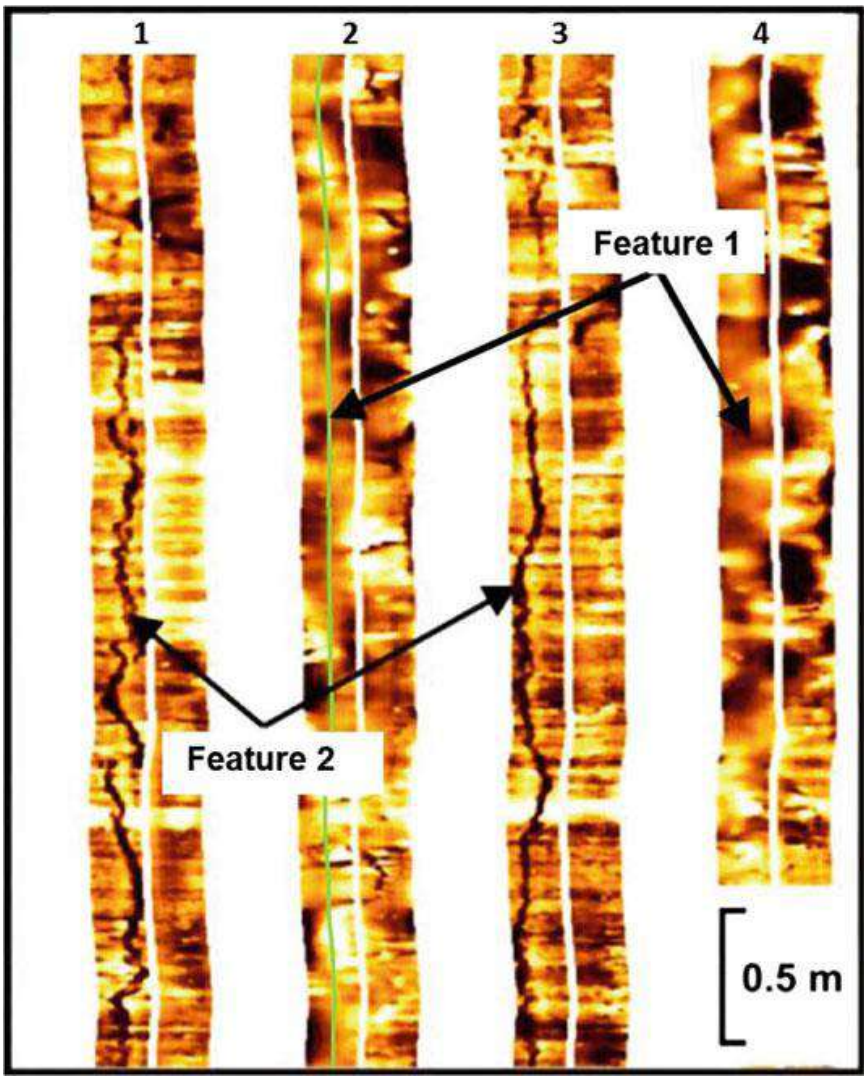

Fig. 7 Four pads of an image log display two prominent features in alternate pads. The darker layers represent conductive bodies and lighter colour the resistive features. 'Feature 1' appears to be broad and blur and can be seen in pads 2 and 4. 'Feature 2' is a linear, narrow feature running parallel along pads 1 and 3 (Reproduced from Tingay et al. 2008)

Answers:

a. Using Eqs. (2) and (3), $S_{\mathrm{Hmax}} = 210.4$ MPa and $S_{\mathrm{hmin}} = 49.4$ MPa.

b. Since S_{hmin} is the least principal stress, S_{Hmax} cannot be less than S_{hmin}. So, the lower bound of S_{Hmax} is $= 61.5$ MPa. The upper bound is unconstrained: either $<$ or $> S_{\mathrm{v}}$. A normal fault regime is characterized $S_{\mathrm{hmin}} < S_{\mathrm{Hmax}} < S_{\mathrm{v}}$. Here, S_{v} is the maximum principal stress. If S_{Hmax} is $> S_{\mathrm{v}}$, i.e. $S_{\mathrm{hmin}} < S_{\mathrm{v}} < S_{\mathrm{Hmax}}$, then it is in strike-slip regime. Thus, two stress regimes are possible.

4 Conclusions

Modern-day logging tools aid in identifying the features related to geomechanical issues. Kingdon et al. (2016) while studying the in situ stress for the shales state that before determining the stresses from any laboratory tests, high-resolution image logs should reliably determine the stress orientations. DIFs and breakouts are the features obtained from image log analysis. Such fracturing and breakouts happen due to compressive failures in the borehole and the orientation of the stress directions can be obtained by studying these features. DIFs oriented parallel to the S_{Hmax} direction, and the breakout formation gives the S_{hmin} direction.

Acknowledgements Ake Fagereng and Andrea Billi provided detailed comments in multiple rounds, when this article was submitted in a different platform. While we acknowledge their strong efforts, we need to state that we have not been able to accommodate all of their comments. *No data was taken from Reliance Industries Limited*. For more geo-mechanical discussions, see Patil (2015).

Appendix

Table 1 List of electrical logs (Rider 2011; Tingay et al. 2008)

Trade name	Company name	Number of pads
Electrical Micro Imaging Tool (EMI)	Halliburton	6
Formation Micro Scanner (FMS)	Schlumberger	4
Formation Micro Imager (FMI)	Schlumberger	8
Oil-based Micro Imager (OBMI)	Schlumberger	4/8
Simultaneous Acoustic and Resistivity Imager (STAR)	Baker Hughes	6

Table 2 List of acoustic logs (Rider 2011; Tingay et al. 2008)

Trade name	Company name
Circumferential Acoustic Scanning Tool (CAST)	Halliburton
Ultrasonic Borehole Imager (UBI)	Schlumberger
Simultaneous Acoustic and Resistivity Imager (STAR)	Baker Hughes
Circumferential Borehole Imaging Log (CBIL)	Baker Hughes

References

Anderson EM (1905) The dynamics of faulting. Trans Edinb Geol Soc 8:387–402
Bailey A, Tenthorey E, Ayling B (2017) Characterising the present-day stress regime of the Georgina Basin. Aust J Earth Sci 64:121–136
Barton CA, Zoback MD (2002) Wellbore imaging technologies applied to reservoir geomechanics and environmental engineering. In: Lovell M, Parkinson N (eds) Geological applications of well logs: AAPG Methods in Exploration, vol 13, p. 229–239
Bell JS, Gough DI (1979) Northeast-Southwest compressive stress in Alberta: evidence from oil wells. Earth Planet Sci Lett 45:475–482
Bell JS (1996) Petro geoscience 1. In situ stresses in sedimentary rocks (Part 1): measurement Techniques. Geosci Can 23:85–100
Bell JS (2003) Practical methods for estimating in situ stresses for borehole stability applications in sedimentary basins. J Petrol Sci Eng 38:111–119
Brochure OBMI (2006) Borehole imaging in oil based mud. Schlumberger Ltd., Sugarland TX
Byerlee JD (1978) Friction of rock. Pure appl Geophys 116:615–626
Chatterjee R, Singha DK (2018) Stress orientation from image log and estimation of shear wave velocity using multiple regression model: a case study from Krishna—Godavari basin, India. J Indian Geophys Union 22:128–137
Dasgupta S, Dasgupta T, Singh VN, Mukherjee S (2018) A numerical study of the effect of borehole on the response of epithermal neutron log. In: Fagereng A, Billi A (eds) Problems and solutions in structural geology and tectonics. Mukherjee S (ed) Developments in structural geology and tectonics book series. Elsevier ISSN: 2542–9000
De Bree P, Walters JV (1989) Micro/minifrac test procedures and interpretation for in situ stress determination. Int J Rock Mech Min Sci Geomech Abstr 26(6):515–521
Fellgett MW, Kingdon A, Williams JDO, Gent CMA (2018) Stress magnitudes across UK regions: new analysis and legacy data across potentially prospective unconventional resource areas. Mar Pet Geol 97:24–31
FMI Brochure (2002) Borehole geology, geomechanics and 3D reservoir modeling. Schlumberger
Fossen H (2016) Structural geology, 2nd edn. Cambridge University Press, pp 1–510 (ISBN 978-1-107-05764-7)
Fowler MJ, Weir FM (2008) The use of borehole breakout for geotechnical investigation of an open pit mine. In: Potvin Y, Carter J, Dyskin A, Jeffrey R (eds) SHRMS 2008. Australian Centre for Geomechanics. Perth (ISBN 978-0-9804185-5-2)
Gough DI, Bell JS (1981) Stress orientation from oil well fractures in Alberta and Texas. Can J Earth Sci 18:1458–1370
Hillis RR, Reynolds SD (2000) The Australian stress map. Journal of the Geological Society 157:915–921
Hurley N (2004) Borehole images. In: Asquith G, Krygowski D (eds) Basic well log analysis: AAPG methods in exploration, vol 16, pp 151–163
Kingdon A, Fellgett M, Williams J (2016) Use of borehole imaging to improve understanding of the in- situ stress orientation of Central and Northern England and its implications for unconventional hydrocarbon resources. Mar Pet Geol 73:1–20
Labuz JF, Zang A (2012) Mohr-coulomb failure criterion. Rock Mech Rock Eng 45:975–979
Lai J, Wang G, Wang S, Cao J, Li M, Pang X, Han C, Fan X, Yang L, He Z, Qin Z (2018) A review on the applications of image logs in structural analysis and sedimentary characterization. Mar Pet Geol 95:139–166
Lin W, Yamamoto K, Ito H, Masago H, Kawamura Y (2008) Estimation of minimum principal stress from an extended leak-off test onboard the chikyu drilling vessel and suggestions for future test procedures. Sci Drill 6:43–47
Mukherjee S (2013) Channel flow extrusion model to constrain dynamic viscosity and Prandtl number of the Higher Himalayan Shear Zone. Int J Earth Sci 102:1811–1835

Mulchrone KF, Mukherjee S (2016) Kinematics and shear heat pattern of ductile simple shear zones with 'slip boundary condition'. Int J Earth Sci 105:1015–1020

Nelson EJ, Meyer JJ, Hillis RR, Mildren SD (2005) Transverse drilling-induced tensile fractures in the West Tuna area, Gippsland Basin, Australia: implications for the in situ stress regime. Int J Rock Mech Min Sci 42:361–371

Nian T, Wang G, Xiao C, Zhou L, Deng L, Li R (2016) The in situ stress determination from borehole image logs in the Kuqa depression. J Nat Gas Eng 34:1077–1084

Patil M (2015) Dipmeter surveys in petroleum exploration. BS Publications. Hyderabad, pp 1–128. ISBN: 978-93-83635-25-2.

Prensky SE (1999) Advances in borehole imaging technology and applications. In: Lovell M, Williamson G, Harvey P (eds) Borehole imaging: applications and case histories, vol 159. Geological Society Special Publication, pp 1–43

Rajabi M, Tingay M, King R, Heidbach O (2017) Present-day stress orientation in the Clarence-Moreton Basin of New South Wales, Australia: a new high density dataset reveals local stress rotations. Basin Res 29:622–640

Richardson NJ, Richards FL, Rippington SJ, Bond CE, Wilson RW (2015) Industrial structural geology: principles, techniques and integration: an introduction. In: Richardson NJ, Richards FL, Rippington SJ, Bond CE, Wilson RW (eds) Industrial structural geology: principles, techniques and integration, vol 421. Geological Society, London, Special Publications, pp 1–5

Rider M (2011) The geological interpretation of well logs, 2nd edn. Whittles Publishing, Caithness. ISBN 0954190688

Thorsen K (2011) In situ stress estimation using borehole failures-even for inclined stress tensor. J Petrol Sci Eng 79:86–100

Tingay M, Reinecker J, Műller B (2008) Borehole breakout and drilling -induced fracture analysis from image logs. In: World stress map project guidelines: image logs. http://dc-app3-14.gfz-potsdam.de/pub/guidelines/WSM_analysis_guideline_breakout_image.pdf. Accessed on 12 Mar 2018

Zoback MD (2007) Reservoir geomechanics. Cambridge University Press, Cambridge, pp 1–445 (ISBN 978-0-521-77069-9)

Zoback MD, Moos D, Mastin L (1985) Well Bore Breakouts and in situ stress. J Geophys Res 90:5523–5530

Zoback ML (1992) First- and second-order patterns of stress in the lithosphere: the world stress map project. J Geophys Res Solid Earth 97:11703–11728